ACCELERON AEROSPACE JOURNAL (AAJ)
E-ISSN: 2583-9942 (Online) | Accessible at www.acceleron.org.in
Volume 6, Issue 3, (pp.1745-1756)
Article ID: AAJ.11.2106-2611
Research Paper
https://doi.org/10.61359/11.2106-2611

Numerical Study on the Change of Aerodynamic Characteristics of Rotors Due to Ice Accretion Depending on the Sectional Shapes

Hoonjae Kim [1*], Hojun Jang [2†], Byoungsoo Kim [3‡]

[1]MS Student, Department of Aerospace Engineering, Chungnam National University, Daejeon, Republic of Korea

[2]PhD Student, Department of Aerospace Engineering, Chungnam National University, Daejeon, Republic of Korea

[3]Professor, Department of Aerospace Engineering, Chungnam National University, Daejeon, Republic of Korea

Abstract: Aircraft are frequently exposed to various atmospheric conditions during ascent, where they encounter supercooled droplets within clouds. These droplets can freeze upon contact with the aircraft surface, leading to ice accretion at temperatures below the freezing point. This ice formation alters the aircraft's shape, adversely affecting its aerodynamic properties, flight efficiency, and stability. This study investigates the effects of icing on airfoil geometries, focusing on the aerodynamic characteristics and robustness of rotor blades in icing conditions through two-dimensional simulations and the Blade Element Momentum (BEM) method. Our findings indicate that an increase in the thickness ratio within the same camber series leads to reduced maximum droplet collection efficiency and broadens the range of the impingement limit for supercooled droplets. This effect is pronounced as thicker airfoils show lesser ice accumulation, enhancing aerodynamic stability under icing conditions. Conversely, airfoils with a lower camber ratio exhibit decreased maximum collection efficiency and a milder slope of droplet collection efficiency, resulting in reduced thrust loss. This suggests that selecting airfoil profiles with a lower camber ratio and greater thickness can significantly improve the robustness against icing conditions.

Table of Contents

1. Introduction

Aircraft primarily conduct ascent flights from the ground level, continuously increasing their operating altitude while being exposed to various meteorological conditions. As the altitude increases, the atmospheric temperature drops below the freezing point, causing supercooled droplets within clouds to adhere to the aircraft surface and initiate ice accretion. This ice formation alters the shape of the aircraft, thereby impairing its aerodynamic properties and negatively affecting flight efficiency and stability. Notable examples of accidents caused by icing include the incidents of American Eagle Flight 4184 in 1994 and Comair Flight 3272 in 1997, where ice accretion on the wings, induced by cold external conditions, weakened the aerodynamic performance of the aircraft. Thus, ice accretion is a critical variable to consider in the operation of aircraft [1].

Particularly, research on rotor icing is essential during the design phase of high-altitude unmanned aerial vehicles (UAVs) that fly at high altitudes. High-altitude UAVs ascend at lower rotational speeds in mid-altitudes to reach higher operational altitudes. This flight environment exposes them to icing conditions characterized by lower Reynolds numbers compared to conventional aircraft. Consequently, modern high-altitude UAVs are equipped with de-icing systems and ice detection sensors to mitigate the frequent exposure to such conditions. The addition of these systems, however, increases the weight of the aircraft and reduces flight efficiency.

Previous studies on icing, involving both numerical and experimental research, have been actively pursued internationally.[2,3,4] A. Baumert et. al have reported that results from numerical studies and wind tunnel experiments are complementary, indicating mutual support for findings related to icing effects.[3] S. Yan also conducted experimental studies on the performance changes of UAV rotors exposed to icing environments, finding a linear correlation between power increase, thrust decrease, and icing duration.[4] Domestically, the Lattice Boltzmann Method (LBM) has been used to analyze flow and noise characteristics arising in multi-airfoil

*MS Student, Dept. of Aerospace Engineering, Chungnam National University, Daejeon, Republic of Korea.
†PhD Student, Dept. of Aerospace Engineering, Chungnam National University, Daejeon, Republic of Korea.
‡Professor, Dept. of Aerospace Engineering, Chungnam National University, Daejeon, Republic of Korea. **Corresponding Author:** kbskbs@cnu.ac.kr.
Article History: Received: 08-Feb-2026 || Revised: 24-Mar-2026 || Accepted: 24-Mar-2026 || Published Online: 31-March-2026.

configurations due to icing. These studies have shown that icing can reduce noise at specific angles of attack.[5] Additionally, experimental studies on the aerodynamic performance of rotating rotors in various icing conditions have been performed.[6] Despite the extensive experimental and theoretical research, studies on performance changes in rotors due to different airfoil shapes under icing conditions remain insufficient. This study aims to examine the changes in aerodynamic characteristics of iced rotor blades based on the cross-sectional shape of the airfoil in actual icing conditions. Using the Blade Element Momentum (BEM) method,[7] it predicts changes in the aerodynamic performance of iced rotor blades and explores the design of rotors with high robustness to icing.

2. Numerical Approach Verification

2.1 Flow Field Analysis Verification

2.1.1 Analysis Method

Prior to performing ice accretion analysis, a three-dimensional flow analysis must be conducted, which then forms the basis for subsequent ice accretion studies, including reliability verification. In this study, flow field validation was carried out using airfoil profiles of wind turbine blades, specifically the S809, and helicopter blades using the NACA23012 profile. Numerical results were compared with experimental outcomes to validate the flow field. ANSYS FLUENT (2022 R1) was utilized for flow analysis, employing the Spalart-Allmaras turbulence model, selected for its simplicity and high accuracy in computations.[8]

2.1.2 Grid and Flow Conditions

For the flow field analysis, the shape and grid of the airfoil were generated using the in-house code eGwing. Figure 1 illustrates the flow field analysis grid, and Figure 2 shows the flow conditions. The external grid was set such that the inlet and the boundary conditions above and below the airfoil were 15 times and the outlet 25 times the chord length from the airfoil's trailing edge. The height of the first cell was set to maintain a y+ value conducive to accurate results, and an inflation ratio of 1.15 was used to create 170,000 structured grids. Energy equations were employed for subsequent ice analysis, and the Pressure far-field approach was used for the analyses. Table 1 organizes the flow analysis conditions.

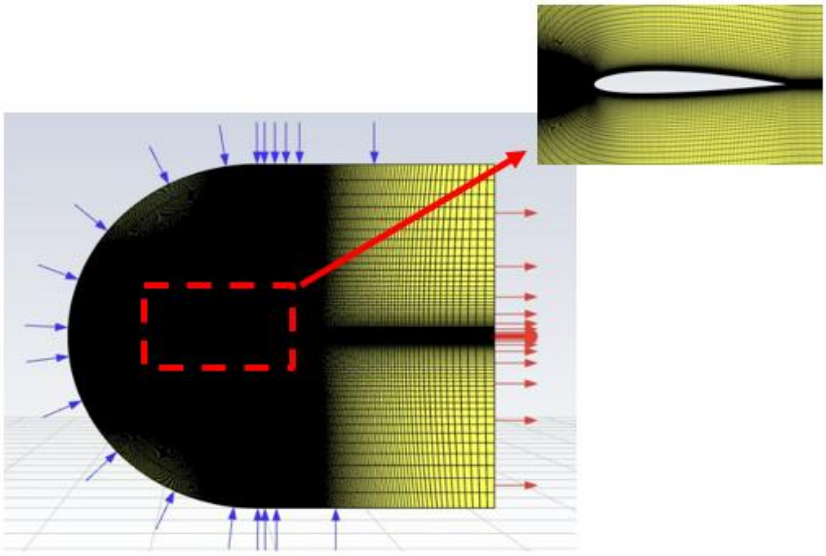

Figure 1. Airfoil Geometry and Mesh

Acceleron Aerospace Journal || AAJ.11.2106-2611
Volume 6, Issue 3, pp (1745-1756)
E-ISSN- 2583-9942
https://dx.doi.org/10.61359/11.2106-2611

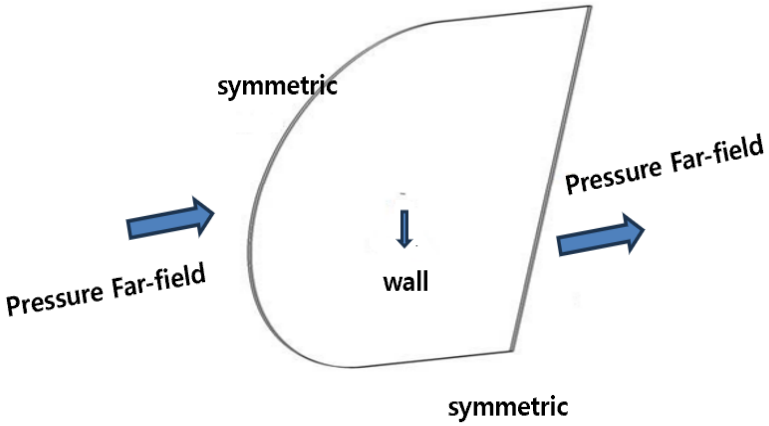

Figure 2. Boundary Conditions

Table 1. Airfoils and Analysis Conditions

Contents	Case 1	Case 2	Case 3
Airfoil	S809		NACA 23012
Nodes	170,000		
Inlet velocity (m/s)	25		78.23
AoA(degree)	4	16	2.5
Air condition	Ideal gas(Pressure Far-field)		

2.1.3 Analysis Results Comparison

The flow field analysis was validated by comparing the coefficient of pressure (Cp) across different angles of attack. Figure 3, Figure 4, and Figure 5 present graphs comparing the flow analysis reliability for the airfoils, with Fluent-derived Cp values showing a deviation within 2% of experimental data,[9] suggesting consistency in data trends. The observed discrepancies are hypothesized to stem from insufficient pre-information about the flow conditions used in the experiments.

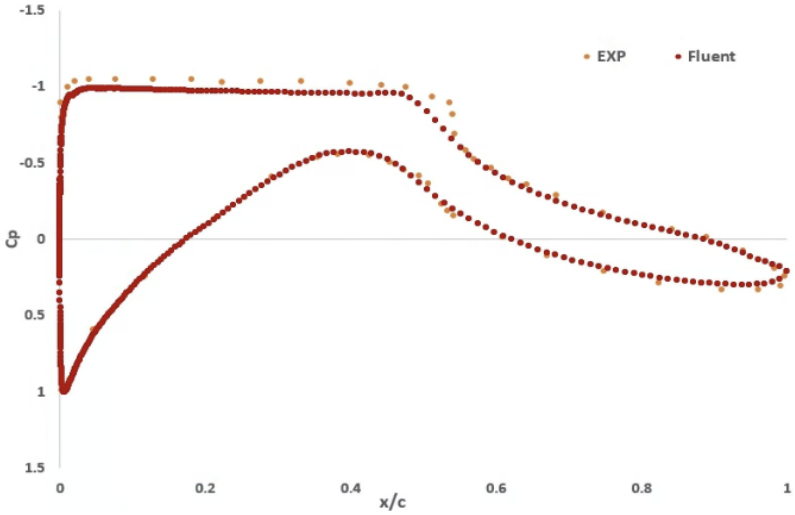

Figure 3. S809 Pressure Coefficient at 4 degrees

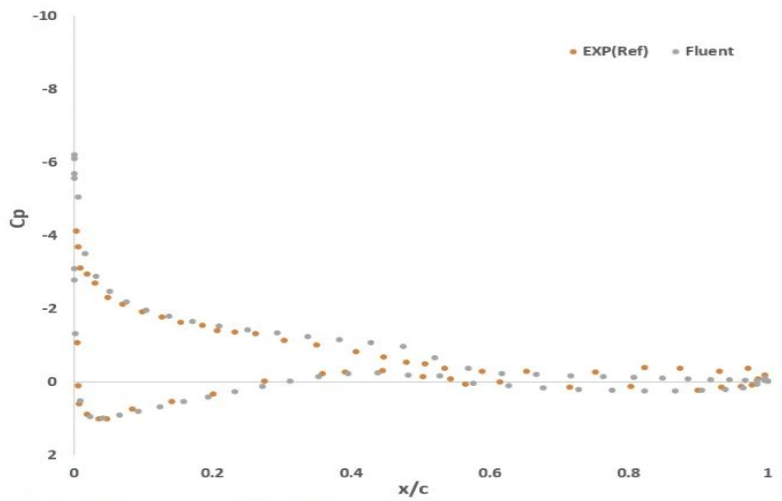

Figure 4. S809 Pressure Coefficient at 16 degrees

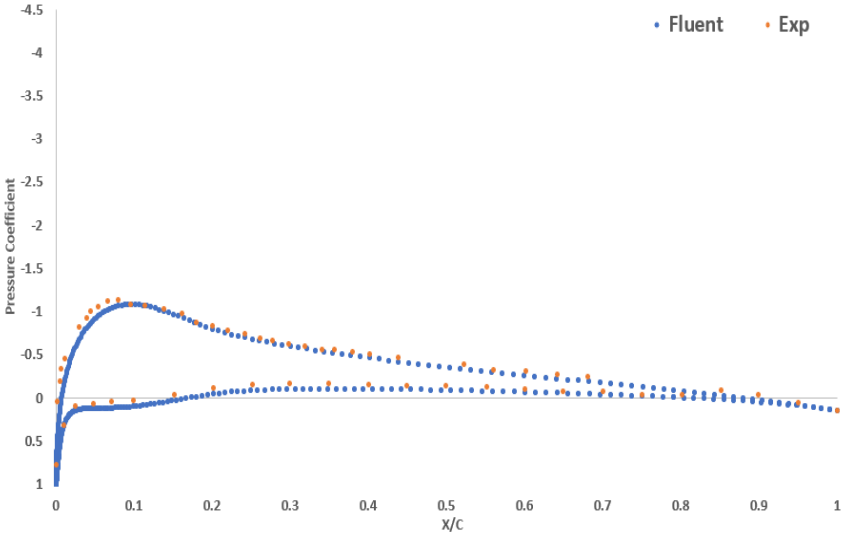

Figure 5. NACA23012 Pressure Coefficient at 2.5 degrees

2.2 Droplet Field Analysis Verification

2.2.1 Analysis Method

Utilizing the results from Section 2.1.3, droplet collection efficiency was calculated to verify the distribution of the droplet field on the airfoil surface. Fensap Ice's Drop3D was employed to define and analyze the size and distribution of supercooled droplets. To expedite the analysis, a monodisperse distribution was used instead of a Lagmuir D distribution for droplet size. The reliability of the droplet field distribution computed by Drop3D was confirmed by comparing the analysis results with numerical and experimental values from the literature for NACA23012.[10]

2.2.2 Results Comparison

Figure 6 presents a graph comparing the droplet collection efficiency analyzed using Drop3D with experimental and numerical values from reference studies. Although discrepancies occurred in the range of the impingement limit value, the maximum collection efficiency matched the experimental data. Discrepancies in the impingement limit values were within a 3% error margin when compared to the numerical results from the literature, likely due to variations in flow input conditions.

Acceleron Aerospace Journal || AAJ.11.2106-2611
Volume 6, Issue 3, pp (1745-1756)
E-ISSN- 2583-9942
https://dx.doi.org/10.61359/11.2106-2611

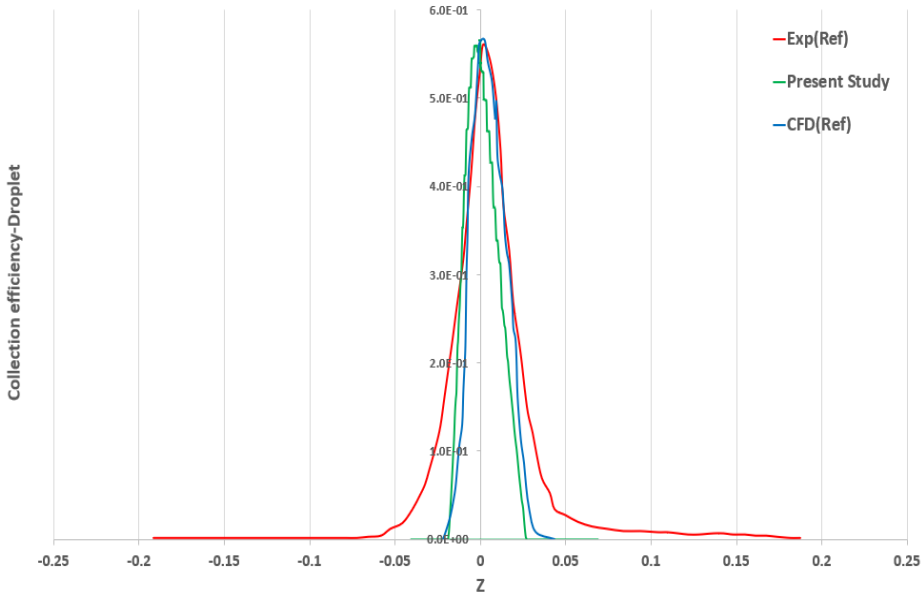

Figure 6. NACA23012 Collection Efficiency at 2.5 degrees

3. Numerical Analysis Results

3.1 Results Based on Airfoil Geometry

The droplet collection efficiency was analyzed based on the sectional shape of the blade airfoils. Figure 7 illustrates the droplet collection efficiency under identical flow conditions for airfoils with and without camber. It was observed that airfoils with camber had a wider impingement limit point compared to symmetrical airfoils, due to stagnation pressure forming on the underside of the airfoil leading to a broader impingement limit distribution. Additionally, cambered airfoils showed a gentler slope in droplet collection efficiency, which resulted in a more gradual ice accretion shape. Figure 8 shows the droplet collection efficiency as a function of thickness ratio under the same flow conditions, revealing that thicker airfoils within the same series had lower maximum collection efficiencies and less ice thickness, along with a broader impingement limit range. This analysis confirms that the airfoil geometry significantly influences the unique droplet collection efficiency and ice shape under identical icing conditions. Irregularities in S809 droplet collection efficiency data were attributed to the limited nodal points defining the shape.

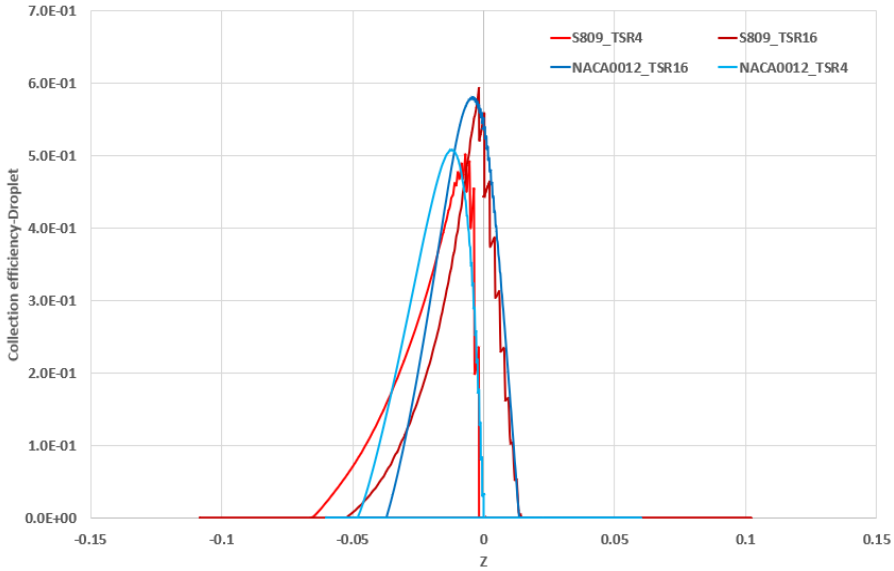

Figure 7. s809 & NACA0012 Collection Efficiency

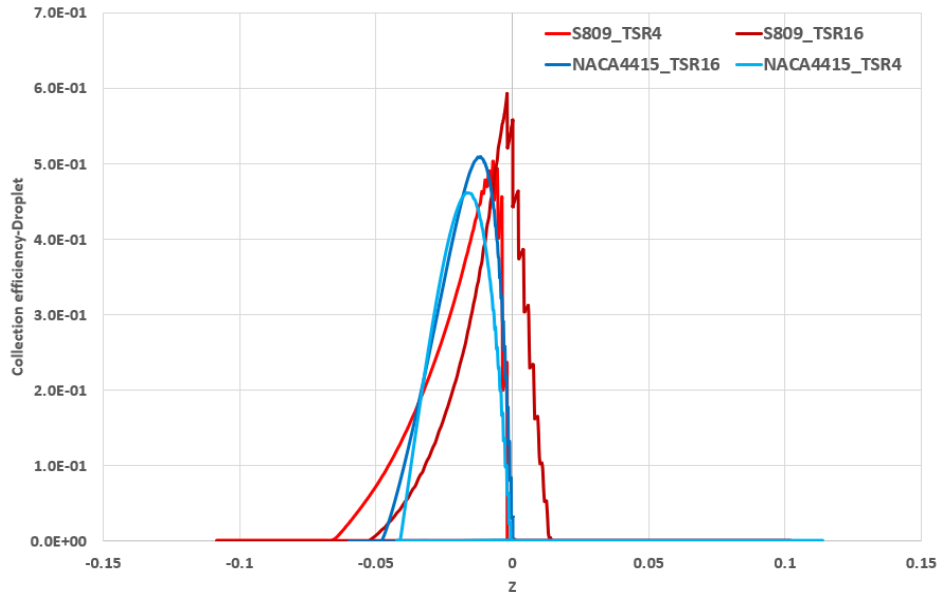

Figure 8. s809 & NACA4415 Collection Efficiency

3.2 Icing Based on Airfoil Position

This study conducted icing analysis based on the blade position at a fixed rotational speed of 1250rpm. Figure 9 shows the shape of a rotor composed of NACA0012 airfoils. From the root to the tip of the blade, the linear velocity increases due to rotation, subsequently increasing the relative velocity. This leads to an increase in ice thickness from the root towards the tip of the blade. Figure 10 presents a graph showing the lift coefficient at various angles of attack depending on the position along the blade, indicating a decrease in lift coefficient and a reduction in stall angle towards the blade tips. This analysis allows for predictions of changes in icing shape and aerodynamic characteristics depending on the position of the airfoil section along the rotor blade.

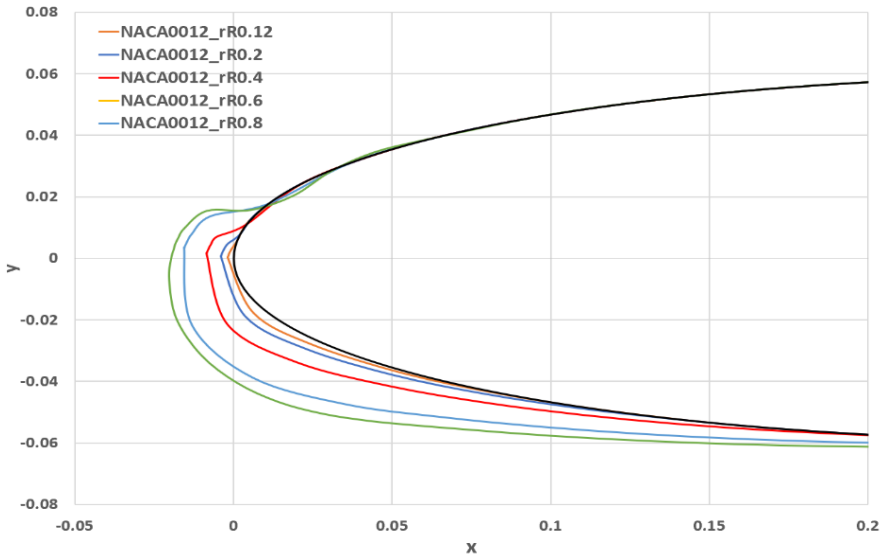

Figure 9. NACA0012 Airfoil shape with icing(r/R)

Acceleron Aerospace Journal || AAJ.11.2106-2611
Volume 6, Issue 3, pp (1745-1756)
E-ISSN- 2583-9942
https://dx.doi.org/10.61359/11.2106-2611

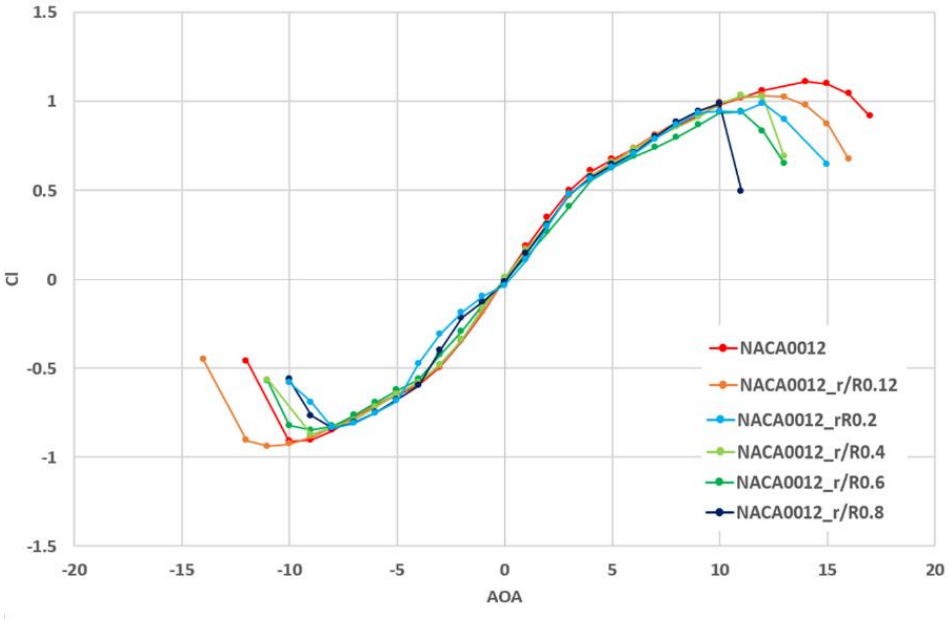

Figure 10. NACA0012 lift coefficient with icing(r/R)

3.3 Icing Based on Airfoil Geometry

3.3.1 Analysis Method

Using the results of the flow analysis of iced blade sections, the three-dimensional aerodynamic characteristics of iced rotors were analyzed using the Blade Element Momentum (BEM) method. The geometry of iced blades was extracted using ICE3D, and the data was then optimized for node count using XFOIL to prepare the geometry for BEM analysis. The modified iced airfoil geometry was analyzed using the commercial software JBLADE to assess the 3D aerodynamic characteristics. Figure 11 illustrates the methodological flow chart for analyzing the iced rotor.

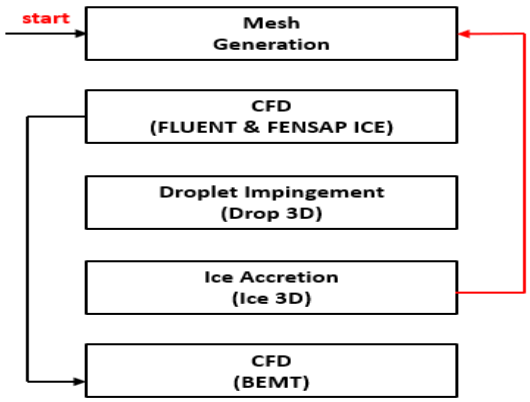

Figure 11. Analysis flow chart

3.3.2 Changes in Aerodynamics Due to Thickness

The aerodynamic characteristics of rotors with varying thickness ratios among symmetrical airfoils were analyzed. Figure 12 shows the changes in rotor thrust due to ice accretion near the leading edge, revealing that thicker airfoils experienced less reduction in thrust due to a decrease in the maximum collection efficiency of supercooled droplets, resulting in reduced ice thickness. This also led to a gentler slope of the thrust reduction ratio. Figure 13 illustrates how the thrust reduction ratio increases with inflow velocity, indicating that thicker airfoils result in less reduction in thrust. Figure 14 shows a graph of the rotor torque due to ice accretion at various inflow speeds, with iced rotor shapes showing higher torque requirements compared to the original rotor shape.

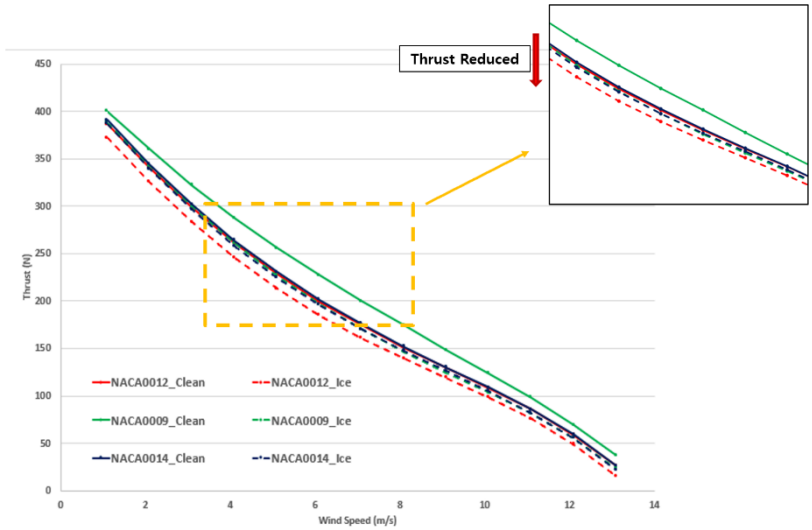

Figure 12. Symmetry airfoil rotor Thrust with icing

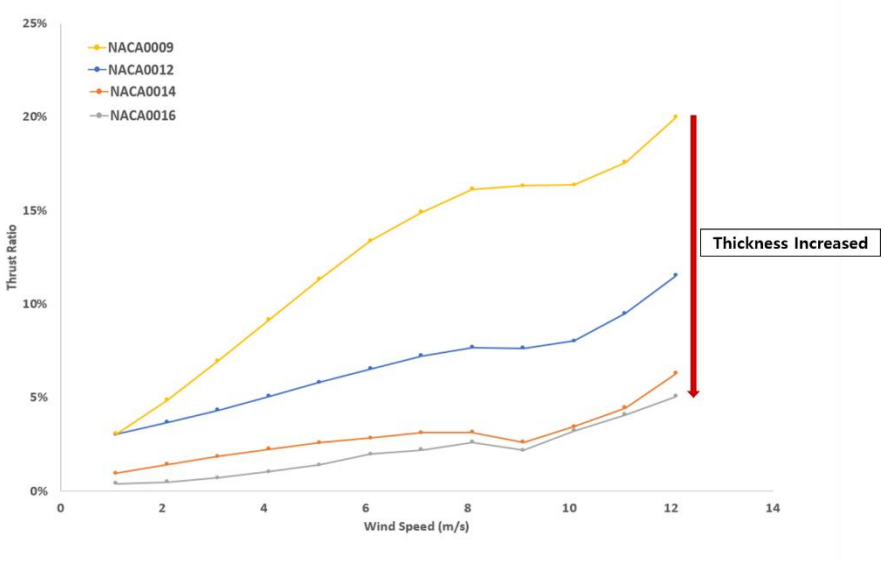

Figure 13. Symmetry airfoil rotor Thrust Ratio with icing

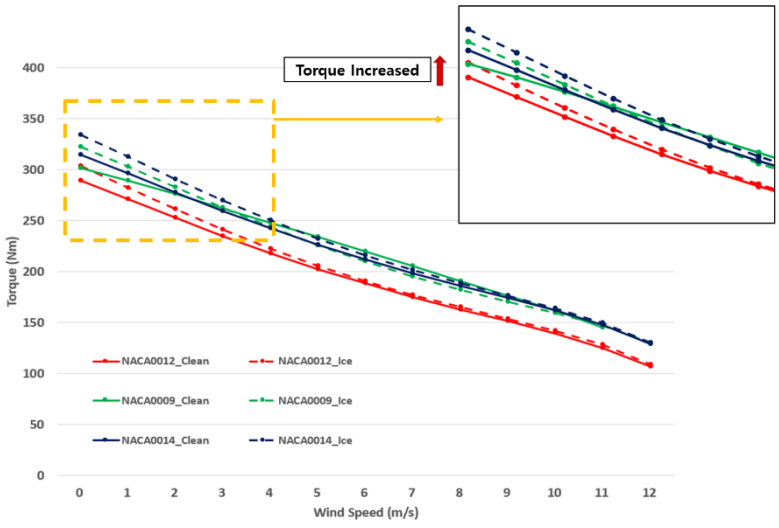

Figure 14. Symmetry Airfoil Rotor Torque with Icing

Acceleron Aerospace Journal || AAJ.11.2106-2611
Volume 6, Issue 3, pp (1745-1756)
E-ISSN- 2583-9942
https://dx.doi.org/10.61359/11.2106-2611

3.3.3 Changes in Aerodynamics Due to Camber

The aerodynamic characteristics of rotors with different camber levels in the same thickness airfoils were analyzed. The thickness was consistently 12%, but the camber radius and degree varied. Figure 15 shows the changes in rotor thrust due to ice accretion at the leading edge of the blade, which reduced thrust. Figure 16 illustrates the thrust reduction ratio with inflow speed for cambered airfoil rotors, showing reduced thrust loss after a certain critical inflow speed, especially for airfoils with less camber. This resulted in a milder gradient of droplet collection efficiency and smaller ice accretion at the blade leading edge, thereby reducing the thrust reduction ratio. Figure 17 shows the rotor torque due to ice accretion in cambered airfoil rotors at various inflow speeds, indicating that cambered rotor shapes require higher torque during operation irrespective of the camber presence.

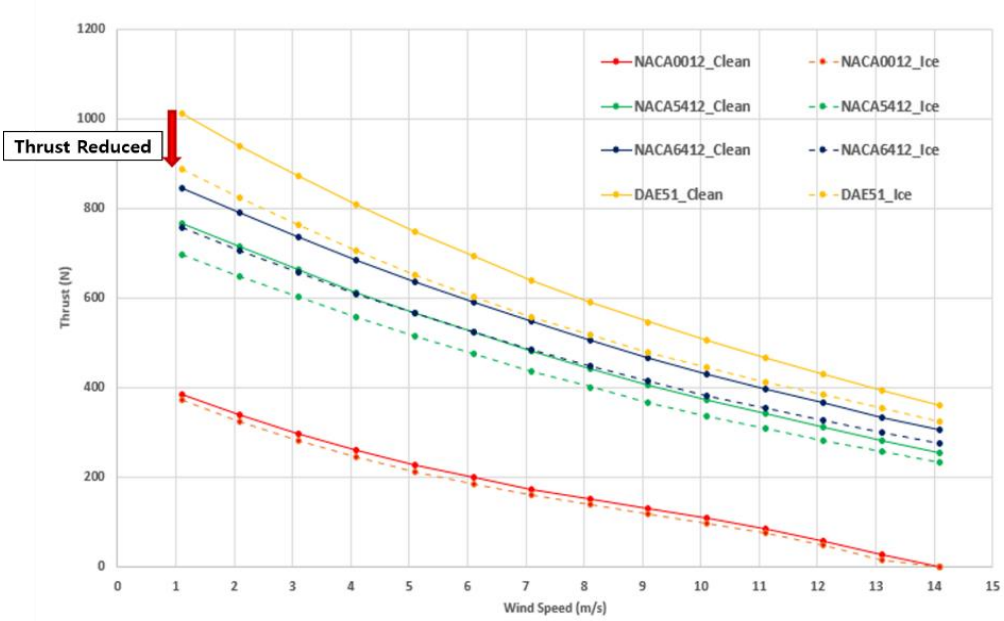

Figure 15. Cambered Airfoil Rotor Thrust with Icing

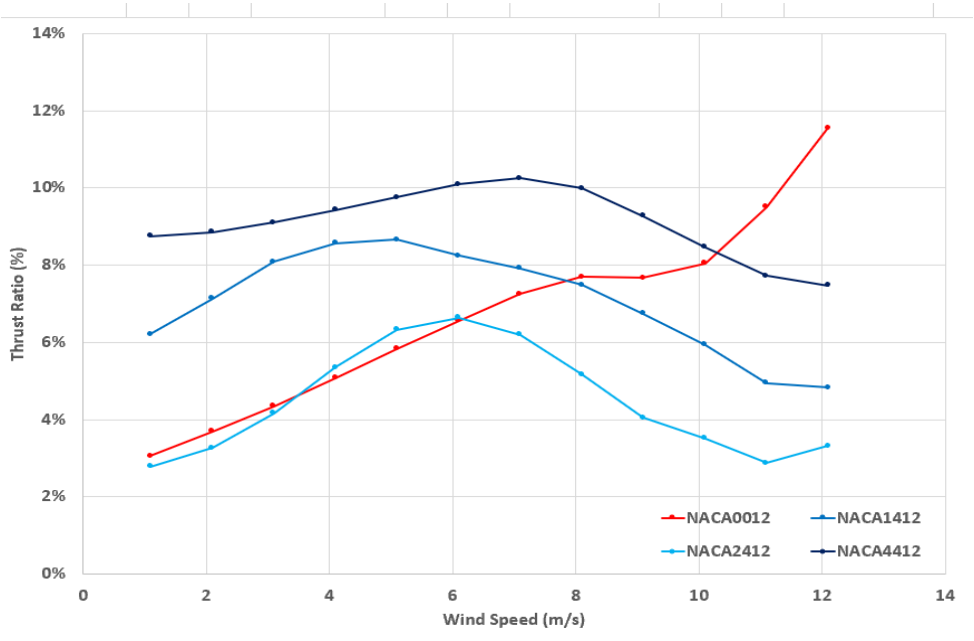

Figure 16. Cambered Airfoil Rotor Thrust Ratio with Icing

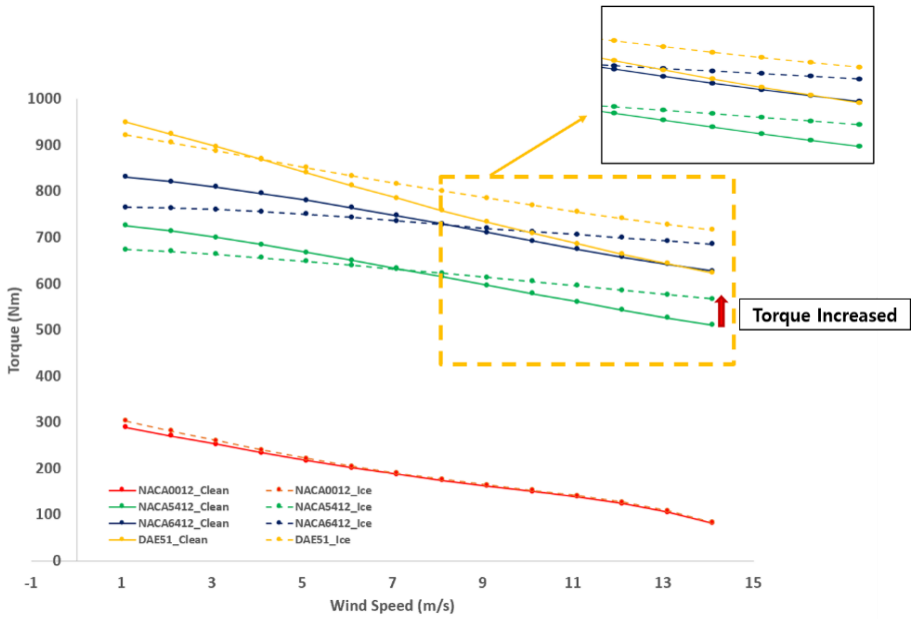

Figure 17. Cambered Airfoil Rotor Torque with Icing

3.3.4 Changes in Aerodynamics Due to Camber and Thickness

Based on the findings from Sections 3.3.2 and 3.3.3, an analysis was conducted on the aerodynamic characteristics of iced rotors concerning variations in airfoil camber and thickness. Figure 18 depicts the graph of thrust changes for iced rotors with a cambered airfoil section having a thickness ratio of 9%. It was observed that the thrust of the iced rotor decreased compared to its original configuration. Figure 19 illustrates the thrust reduction ratio among airfoils of the same camber series but with different thickness ratios. Airfoils with a thickness ratio of 12% showed a lower maximum droplet collection efficiency compared to those with 9%, following a similar trend as seen with symmetrical airfoils. This analysis confirms that the combined effects of camber and thickness significantly influence the aerodynamic performance of rotors under icing conditions.

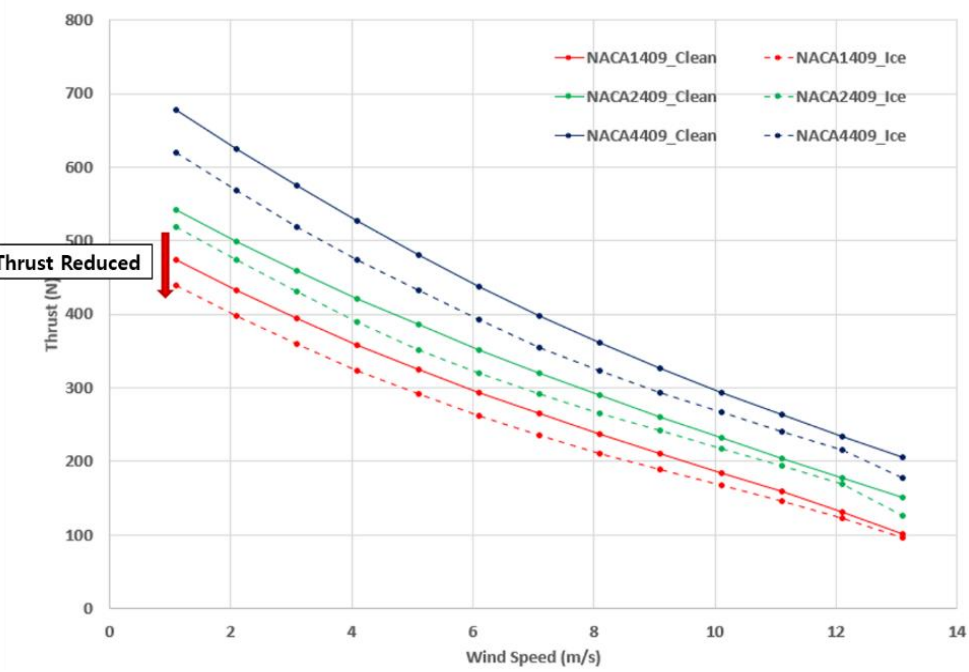

Figure 18. Cambered Airfoil Rotor Thrust with Icing

Acceleron Aerospace Journal || AAJ.11.2106-2611
Volume 6, Issue 3, pp (1745-1756)
E-ISSN- 2583-9942
https://dx.doi.org/10.61359/11.2106-2611

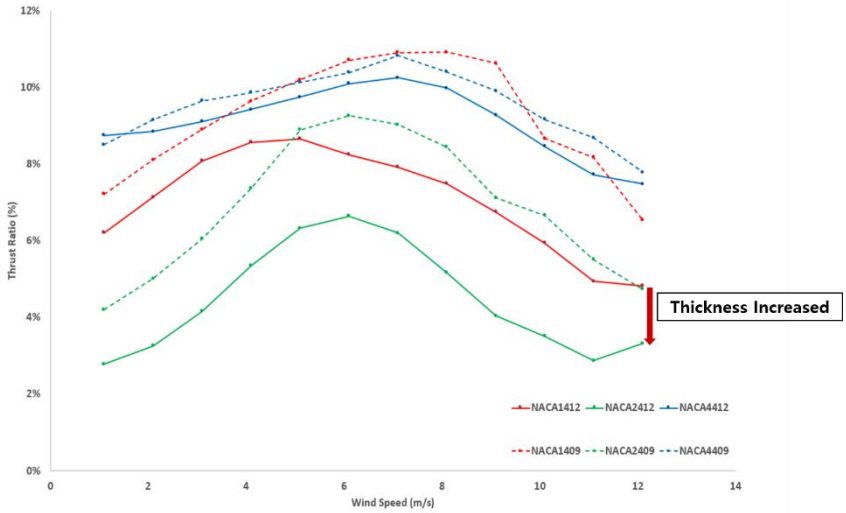

Figure 19. Cambered & Thickness airfoil rotor Thrust with icing

4. Conclusion

This paper has presented the results of two-dimensional icing simulations on airfoil shapes, examining changes in ice accretion shapes and aerodynamic characteristics, and conducted a robustness analysis of the airfoil profiles using the Blade Element Momentum (BEM) method. These analyses enabled the identification of droplet field distributions along the lengthwise position of rotor blades in icing conditions and the prediction of changes in three-dimensional aerodynamic performance. It was observed that an increase in thickness ratio within the same camber series results in a decrease in maximum collection efficiency and an expansion of the impingement limit range for supercooled droplets. Conversely, a lower camber ratio within the same thickness series leads to a reduction in maximum collection efficiency and a milder slope of the droplet collection efficiency. This, in turn, results in a decrease in the thrust reduction ratio as the camber ratio of the airfoil section decreases. These findings suggest that for designing rotors with high robustness to icing conditions, it is advantageous to select airfoil profiles with a lower camber ratio and a thicker profile. Based on these results, further research involving various blade airfoil icing analyses and wind tunnel experiments can be utilized to design rotors with enhanced robustness, minimizing errors and optimizing performance reliability in actual rotors.

5. References

[1] Lee, J. W., Cho, M. Y., Kim, Y. H., Yee, K., & Myong, R. S. (2020). Current status and prospect of aircraft ice protection systems. Journal of the Korean Society for Aeronautical & Space Sciences, 48, 911–925. https://doi.org/10.5139/jksas.2020.48.11.911.

[2] Cao, Y., Zhang, Q., & Sheridan, J. (2008). Numerical simulation of rime ice accretions on an aerofoil using an Eulerian method. The Aeronautical Journal, 112(1131), 243–249. https://doi.org/10.1017/S0001924000002189.

[3] Baumert, A., Bansmer, S., Trontin, P., & Villedieu, P. (2018). Experimental and numerical investigations on aircraft icing at mixed phase conditions. International Journal of Heat and Mass Transfer, 123, 957–978. https://doi.org/10.1016/j.ijheatmasstransfer.2018.02.008.

[4] Yan, S., Opazo, T., Palacios, J., Langelaan, J. W., & Germain, L. D. (2018). Experimental evaluation of multi-rotor UAV operation under icing conditions. Annual Forum Proceedings - AHS International.

[5] Lee, H. J., Kang, M. J., Kim, S., Myong, R. S., & Lee, H. (2023). Numerical investigation of aerodynamic and noise characteristics of an iced multi-element airfoil. Journal of the Korean Society for Aeronautical & Space Sciences, 51, 371–382. https://doi.org/10.5139/JKSAS.2023.51.6.371.

[6] Park, J. H., & Myong, R. S. (2014). Atmospheric icing effects on the aerodynamic characteristics and performance of wind turbine blade. Journal of the Korean Society for Aeronautical & Space Sciences, 42(2), 134–143. https://doi.org/10.5139/JKSAS.2014.42.2.134.

[7] Morgado, J., Silvestre, M. Â. R., & Páscoa, J. C. (2015). Validation of new formulations for propeller analysis. Journal of Propulsion and Power, 31, 467–477. https://doi.org/10.2514/1.B35240.

[8] Ansys Inc. (2022). Ansys Fluent user manual.

[9] Jacobs, E. N., & Clay, W. C. (1936). Characteristics of the NACA 23012 airfoil from tests in the full-scale and variable-density tunnels (Report No. 530). https://ntrs.nasa.gov/citations/19930091603.

[10] Papadakis, M., Rachman, A., Wong, S., Yeong, H., Hung, K. E., Vu, G., & Bidwell, C. S. (2007). Water droplet impingement on simulated glaze, mixed, and rime ice accretions. NASA Glenn Research Center. https://ntrs.nasa.gov/citations/20080008874.

6. Conflict of Interest

The authors declare that they have no known competing financial interests or personal relationships that could have appeared to influence the work reported in this paper.

7. Funding

No funding was issued for this research.